ACS PHYSICAL CHEMISTRY Au
AN OPEN ACCESS JOURNAL OF THE AMERICAN CHEMICAL SOCIETY

pubs.acs.org/physchemau
Article

Crystal Lattice-Induced Stress modulates Photoinduced Jahn–Teller Distortion Dynamics

Published as part of ACS Physical Chemistry Au special issue "Ultrafast Spectroscopy of Chemical Transformations".

Vandana Tiwari, Marcus Gallagher-Jones, Hyein Hwang, Hong-Guang Duan, Angus I. Kirkland, R. J. Dwayne Miller,* and Ajay Jha*

Cite This: ACS Phys. Chem Au 2024, 4, 660–668
Read Online
ACCESS | Metrics & More | Article Recommendations | Supporting Information

ABSTRACT: Efficient photoredox chemical transformations are essential to the development of novel, cost-effective, and environmentally friendly synthetic methodologies. The concept of the entatic state in bioinorganic catalysis proposes that a preorganized structural configuration can reduce the energy barriers associated with chemical reactions. This concept provides one of the guiding principles to enhance catalytic efficiency by maintaining high-energy conformations close to the reaction's transition state. Copper(I)-based photocatalysts, recognized for their low toxicity and highly negative oxidation potentials, are of particular interest in entasis studies. In this study, we explore the impact of entasis caused by stress induced by the surrounding lattice on the excited state dynamics of a prototypical copper(I)-based photocatalyst in a single crystal form. Using femtosecond broadband transient absorption spectroscopy, we show that triplet state formation from the entactic state is faster (∼3.9 ps) in crystals compared with solution (∼11.3 ps). The observed faster intersystem crossing in crystals hints toward the possible existence of distorted square planar geometry with higher spin–orbit coupling at the minima of the S_1 state. We further discuss the influence of entasis on vibrationally coherent photoinduced Jahn–Teller distortions. Our findings reveal the photophysical properties of the copper complex under lattice-induced stress, which can be extended to enhance the broader applicability of the entatic state concept in other transition metal systems. Understanding how environmental stress-induced geometric constraints within crystal lattices affect photochemical behavior opens avenues for designing more efficient photocatalytic systems based on transition metals, potentially enhancing their applicability to sustainable chemical synthesis.

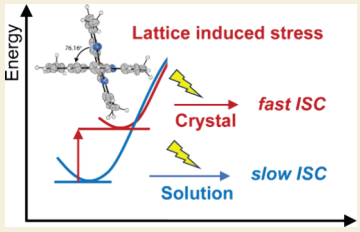

KEYWORDS: *entasis, copper(I)-complex, microED, femtosecond transient absorption, excited state dynamics*

INTRODUCTION

The concept of entasis (a term from architecture) is employed in biochemistry to describe a predistortion of the structure of transition metal complexes at active sites in metalloproteins.[1,2] The structural predistortion inherent in the entactic state of metal complexes suggests a preorganized landscape that lowers the energy barriers for chemical reactions, thereby facilitating more effective and specific catalytic events.[3,4] In bioinorganic chemistry, this principle has generated considerable interest due to its potential for explaining the exceptional efficiency observed in many biological processes that are central to life. Building on fundamental insights gained from studies on metalloproteins, Galperin and Koonin have extended the entasis concept into evolutionary biology.[5] They propose that each emergence of a distinct entactic state at a metal active site marks a crucial evolutionary event, representing substantial advancements that allow organisms to efficiently catalyze a wider array of chemical reactions, providing adaptive benefits within their specific ecologies. The utility of the entactic concept has now transcended its original context within metalloenzymes to provide a broader understanding of enzymatic catalysis.[6] Thus, the entactic state concept provides a malleable framework for exploring evolutionary developments and enzymatic efficiency, with broad implications for both natural and synthetic chemistry.

In transition metal complexes, the enhanced reactivity observed in the entatic geometry is primarily due to elevated energy levels of the reactive and product states relative to the transition state.[4] This conceptual basis is schematically shown in Figure 1a. The associated increase in relative energy levels may be induced by various stressors, such as solvation effects or strains stemming from the configurations of ligand backbones. The systematic investigation of these factors in elevating the energy state of reactants is an active area of ongoing research. Such studies are essential for gaining a

Received: June 24, 2024
Revised: September 15, 2024
Accepted: September 16, 2024
Published: October 2, 2024

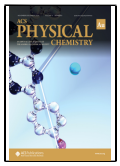

https://doi.org/10.1021/acsphyschemau.4c00047
ACS Phys. Chem Au 2024, 4, 660–668

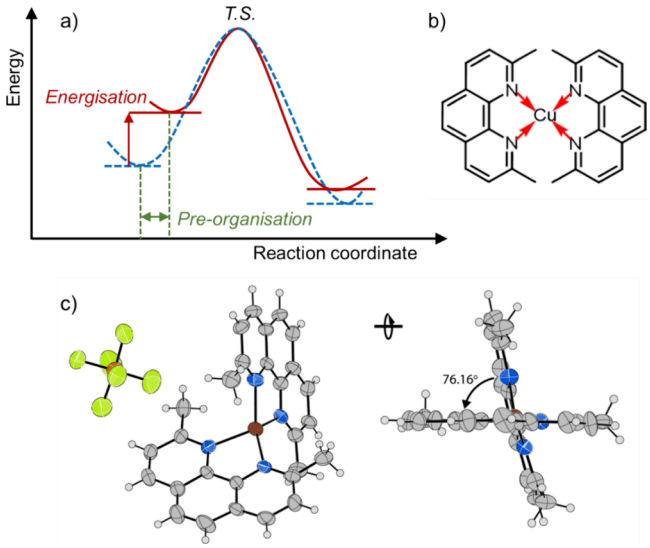

Figure 1. (a) Entasis-induced energization and preorganization of the reactant state: comparing a typical reaction pathway (blue dashed line) vs a reaction where the reactant is modified to stabilize its binding potential, increasing its relative energy levels to the product state and thereby reducing the activation energy (red line). The lower energy barrier induced by entasis facilitates a faster and generally more efficient reaction process. (b) Molecular structure of $[Cu(dmp)_2]^+[PF_6]^-$: bis(2,9-dimethyl-1,10-phenanthroline)copper(I)-hexafluorophosphate. (c) ORTEP representation of the crystal structure of the $[Cu(dmp)_2]^+[PF_6]^-$ complex obtained using microcrystal electron diffraction (microED).

deeper understanding of how these stresses and strains can be effectively harnessed to fine-tune the reactivity of transition metal complexes. By optimizing these interactions, the goal is to expand the utility of entatic states in catalytic systems and other chemical transformations, potentially leading to more efficient and selective processes in industrial and environmental applications.

Copper complexes, which frequently emulate the characteristics of blue copper proteins known for their efficient electron transfer properties,[7−9] are thought to derive their electron transfer efficiency from the entatic state by shuttling between Cu(I) and Cu(II) redox states with minimized reorganization energies. Consequently, copper-based systems are of interest in studies of factors giving rise to entasis and new means of control of reaction dynamics. Innovative ligands have been designed to deliberately introduce strain into Cu(II/I) model complexes, facilitating detailed investigations into the entatic state.[10−15] These efforts aim to understand how induced geometric strain, or lattice coupling, influences the electronic structure and reactivity of copper centers, thereby shedding light on the fundamental principles governing their behavior in biological and synthetic systems. Notably, Dahl and Szymczak have demonstrated that intramolecular H-bonding can tune the primary coordination geometry of a Cu(I) complex in which the H-bond strength to metal-bound halides (Cl, Br, and I) dictates the geometry, with Cu(I)Cl adopting a unique square-planar structure.[16] This H-bonding stabilizes the entatic state, resulting in nearly identical geometries for Cu(I) and Cu(II) on oxidation. Fast electron transfer rates (10^5 M^{-1} s^{-1}) are achieved by minimizing structural reorganization rather than a specific geometry. Similarly, Policar et al. have designed sugar-based epimeric glycol-ligands that are preorganized in water specifically for the Cu(II) oxidation state but are also applicable to Cu(I).[17] Furthermore, Herres-Pawlis et al. have investigated using time-resolved spectroscopy and density functional theory calculations a series of bis(chelate) Cu(I) and Cu(II) guanidine-quinoline complex cations that exhibit a constrained ligand geometry, exhibiting rapid metal-to-ligand charge-transfer dynamics.[10,18] This study also explores how ligand-induced strain influences the structural evolution of these complexes in their excited states. A newly designed homoleptic copper(I) complex reported by Gimeno et al. has also exhibited increased stability in DCM solution, utilizing a nonsymmetrical phenanthroline ligand with bulky *tert*-butyl and isopropyl groups.[19] Despite the steric strain, these Cu(I) complexes showed short-lived, weak emission due to multiple deactivation pathways and ligand motion. While these studies emphasize the role of steric strain in inducing the entactic state, the impact of the stress-induced changes, particularly those affecting the dynamics of photoinduced Jahn−Teller (JT) distortions in Cu(I)-based complexes, remains relatively underexplored.

In its crystalline state, the bis(diimine)copper(I)-hexafluorophosphate, $[Cu(dmp)_2]^+[PF_6]^-$, complex has a configuration that is notably pretwisted in the direction of a Cu(II) geometry. This structural trait establishes the complex as an ideal model for investigating the "entatic-state". This phenomenon is attributed to an intrinsic lattice stress that modifies the geometry from the symmetric D_{2d} form, thereby facilitating a photoinduced shift to Cu(II) geometry following excitation through a metal-to-ligand charge transfer transition. This configuration emulates the stress and resulting distortion imposed by proteins on metallic complexes at the active site.[20] Examining this system within a crystalline framework provides crucial insights into how the structural confines of a crystal lattice affect the photophysical properties of a molecule. More specifically, we have examined the excited state dynamics of the $[Cu(dmp)_2]^+[PF_6]^-$ complex in a single crystal environment. Using femtosecond transient absorption measurements, we have captured the altered ultrafast structural dynamics of this complex in crystals compared to in solution. The affected evolution of triplet state in crystals is also discussed. Our approach provides an understanding of the environmental effects relevant to the stabilization and manipulation of the entatic state, providing a clearer picture of the mechanism by which transition metal complexes behave under different physical constraints.

RESULTS

The $[Cu(dmp)_2]^+[PF_6]^-$ complex was synthesized following a previously established protocol,[21] and further details of the synthesis are given in the Materials and Methods Section. Post synthesis, the crystals were further purified by recrystallization in methanol (Figure S1). Purified crystals were then finely ground between two glass microscope slides and subsequently dispersed on an electron microscopy (EM) grid and loaded into a JEOL CryoARM300 operating at 300 kV for microED analysis.[22] The experimental conditions and parameters for this analysis are detailed in the Materials and Methods Section. The crystal structure obtained using microED measurements is shown in Figure 1c, which confirms the formation of a $[Cu(dmp)_2]^+[PF_6]^-$ complex. A summary of the data collection and refinement statistics is provided in the Supplementary Table ST1. Further analysis of the crystal structure revealed that the angle between the ligand molecular planes is 76.16°, deviating from the 90° angle expected for the

https://doi.org/10.1021/acsphyschemau.4c00047
ACS Phys. Chem Au 2024, 4, 660−668

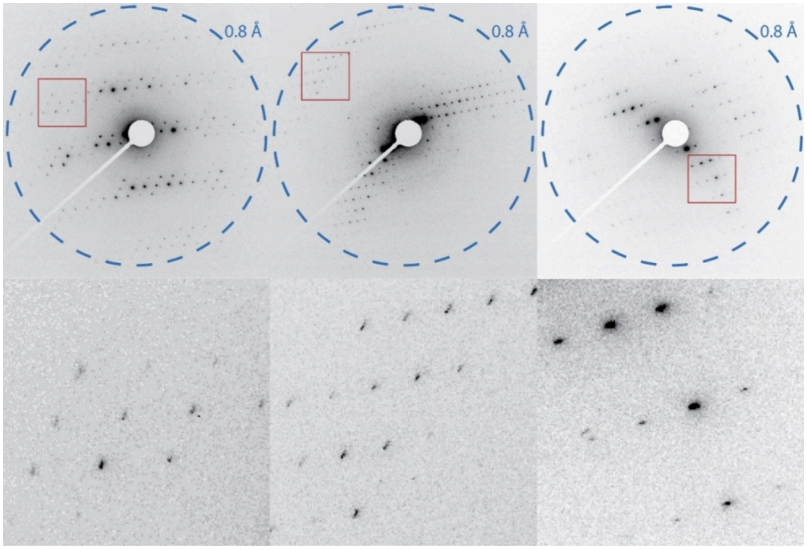

Figure 2. Examples of diffraction patterns captured from $[Cu(dmp)_2]^+[PF_6]^-$ nanocrystals by microED indicating the high resolution diffraction that was achieved. Red boxes indicate the Bragg reflections that show an elliptical skew that may be indicative of strain in the crystal lattice.

D_{2d} symmetry in Cu(I)-based complexes. This deviation is indicative of a predistortion in the $[Cu(dmp)_2]^+$ structure within the crystalline confines. In addition, there are Bragg reflections that are visibly elliptical across all data sets, particularly at high resolution, which is indicative of lattice strain (see Figure 2). This may be due to the crystal lattice resisting the natural 90° orientation of the ligand molecules.

Figure 3a shows the UV−vis absorption spectrum of the complex dissolved in dichloromethane (DCM), in blue, featuring two pronounced absorption bands at approximately 457 nm and a broad spectral shoulder near 530 nm. These spectral features are metal-to-ligand charge transfer (MLCT) transitions.[23] Specifically, the weaker MLCT transition at around 550 nm, described as the A_2 state, aligns with the $S_1 \leftarrow S_0$ transition, which is an optically forbidden transition and the detectable intensity in this band may be attributed to nuclear movements within the S_1 state. In contrast, the stronger absorption band near 454 nm, described as the B_2 state, corresponds to the optically allowed $S_2 \leftarrow S_0$ transition. These spectral designations are supported by findings from time-dependent density functional theory (TDDFT) studies.[24,25] As already described, in the crystalline state, the $[Cu(dmp)_2]^+$ complex exists in a distorted configuration leading to a reduction in symmetry from D_{2d} to D_2.[25] This structural change relaxes the optical selection rules, thereby enhancing the intensity of the $S_1 \leftarrow S_0$ transitions, an effect frequently observed in distorted copper complexes.[24] The absorption spectrum of thin (~400 nm) microtomed slices of the crystal, the blue line in Figure 3a, confirms these predictions (an image of the microtomed crystal is provided in the Supporting Information, Figure S1). The $S_1 \leftarrow S_0$ transition spectral feature is broadened in the crystalline state, although detailed analysis is complicated by the presence of a scattering background. Furthermore, the intense $S_2 \leftarrow S_0$ transition exhibits a shift from 457 nm in the solution phase to 464 nm in the crystalline form, which is attributed to changes in the Franck−Condon overlap due to distortions in the ground state geometry.

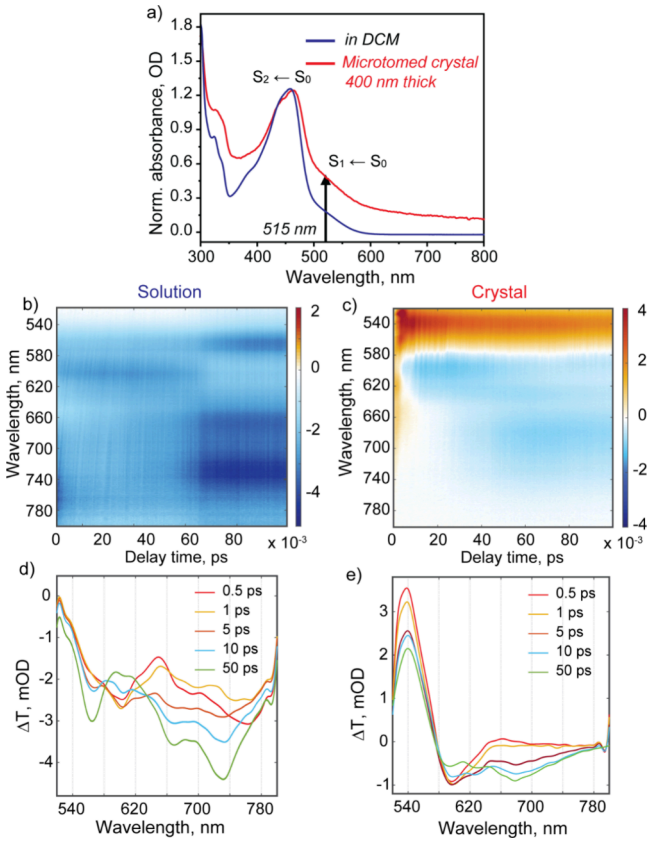

Figure 3. (a) UV−visible absorption spectra of $[Cu(dmp)_2]^+[PF_6]^-$ dissolved in dichloromethane (blue) and 400 nm thin microtomed crystal (red). Transient absorption (TA) spectrum of the copper complex (b) in solution and (c) in a 400 nm thin crystal measured as a function of the time delay between the resonant pump at 515 nm and the visible probe in the range 525−800 nm. The differential transmittance of the probe is shown where positive ΔT represents the ground state bleach (red) and negative ΔT signifies excited state absorption (blue). Differential transmittance spectra at selected temporal delays (0.5, 1, 5, 10, and 50 ps) are also shown for the (d) solution and (e) crystal.

https://doi.org/10.1021/acsphyschemau.4c00047
ACS Phys. Chem Au 2024, 4, 660−668

Transient Absorption Measurements

The ultrafast dynamics of Cu(I)-based complexes have been investigated by several groups using various spectroscopic tools.[25−32] In a study by Tahara et al., femtosecond transient absorption (fs-TA) spectroscopy was used to probe the dynamics of the $[Cu(dmp)_2]^+$ complex following excitation of the MLCT state (S_1) at 550 nm.[27] Their observations delineated two distinct processes: a structural transformation from a D_{2d} (perpendicular) to a D_2 (flattened) configuration and a subsequent intersystem crossing from S_1 to T_1. These processes were shown to occur on distinctly different time scales: ∼0.8 ps for the structural change and ∼10 ps for the intersystem crossing. In our study, we conducted fs-TA measurements on the same Cu(I)-based complex, focusing on both its solution and crystalline states. These measurements were carried out after photoexcitation was induced at a wavelength of 515 nm. This approach allowed us to validate and extend the earlier observed dynamics and provided a comparative insight into how the molecular environment, solvent versus crystal, affects the ultrafast processes in the complex.

Figure 3b shows the fs-TA data from the $[Cu(dmp)_2]^+$ complex in solution following excitation at 515 nm, with selected temporal spectral traces in Figure 3d. The spectral features identified are consistent with those previously reported for this complex. Notably, the excited state absorption (ESA) band at 600 nm observed in the transient spectrum at T = 0.5 ps corresponds to transitions from the S_1 state to higher energy states. Additional ESA bands observed at ∼732, ∼665, and ∼565 nm in the transient spectrum at T = 50 ps are attributed to transitions from the T_1 state to the T_2, T_3, and T_4 states, respectively. The transient absorption spectrum of ∼400 nm thin $[Cu(dmp)_2]^+$ crystals is shown in Figure 3c with spectral evolutions over various time intervals shown in Figure 3e. A prominent feature is the ground state bleach (GSB) at approximately 540 nm, indicative of a more intense $S_1 \leftarrow S_0$ transition in the crystals compared with the solution. This is likely due to structural pretwisting within the crystalline matrix. Immediately following photoexcitation, an ESA feature at ∼595 nm appears, which is assigned to transitions from S_1 to higher energy states. As this band decays, there is an emergence of two ESA bands at 630 and 683 nm, which are interpreted as corresponding to transitions from the T_1 state to the T_2 and T_3 states, respectively.[27] The third high energy ESA band in the crystal data is possibly rendered invisible by the strong ground state bleach. Figure 4 shows a comparative analysis of the triplet state absorption features for both the solution and the crystalline states, revealing a blue shift of these bands in the crystal. This shift suggests a lower triplet state energy in the crystalline form compared to the solution, supporting our hypothesis of crystalline lattice-induced stress on the photophysical properties of the complex.

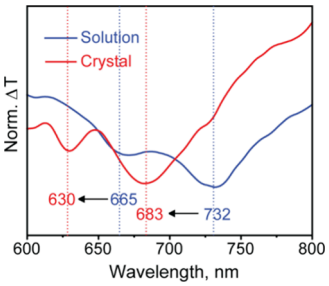

Figure 4. Comparison of the triplet state absorption bands obtained following 20 ps postphotoexcitation in solution (blue) vs crystal (red). The absorption bands in solution centered at 665 and 732 nm are blue-shifted to higher energies centered at 630 and 683 nm in the crystal.

To further elucidate the intricate dynamics observed, each data set was subjected to global analysis.[33] This method allowed the extraction of results, which are represented as species-associated difference spectra (SADS).[34] These spectra explicitly depict the transient species within a coupled rate model framework, thereby clarifying the spectral transitions and elucidating the interactions among various states. Furthermore, the data were interpreted by using a sequential model, implying a progressive evolution of species. This analytical approach not only improves the resolution of intricate spectral data but also supports the development of a more accurate kinetic model for the transient phenomena being investigated. The global fitting results of the solution data are shown in Figure 5a (Figure S2 in the Supporting Information presents quality of the fit). The sequential model is used with three species, and the number of species selection is based on the previously reported models. The first SADS is created immediately after photoexcitation, which reveals ∼730 fs lifetime, shown in Figure 5a as a gray curve. This SADS represents the perpendicular S_1 state. The lifetime of this state is slightly faster than the ∼920 fs observed by Tahara et al.[27] Similarly, the lifetime of the second SADS corresponding to a flattened S_1 state has been extracted as ∼11.3 ps (shown in Figure 5a as a red curve), which is slightly longer than the lifetime of 9.8 ps reported by Tahara et al.[27] This disparity in observed lifetimes may be attributed to differences in the initial photoexcitation energies used in the respective experiments. Specifically, in the current study, the use of a 515 nm excitation wavelength may have provided additional vibrational energy to the S_1 state with different Franck−Condon factors weighting the internal and intersystem crossing transitions, which could account for the variations in the recorded time constants. Similarly, global analysis of the data from the crystalline sample was analyzed to obtain SADS, which are shown in Figure 5b (see Figure S3 in the Supporting Information for quality of the fit). Comprehensive analysis through global fitting of the data indicates that the lifetime of the perpendicular S_1 state is approximately ∼430 fs (SADS in gray, Figure 5b), while the flattened S_1 state exhibits a lifetime of about 3.9 ps (SADS in

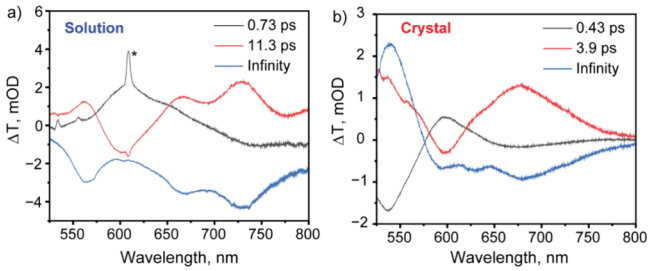

Figure 5. Species-associated difference spectra obtained from the global analysis of the transient absorption data: (a) in DCM solution and (b) crystal. A sequential model is used assuming stepwise evolution of the species. The denotation (*) in the SADS of the solution data corresponds to a Raman frequency of ∼2950 cm^{-1} of the solvent DCM.

https://doi.org/10.1021/acsphyschemau.4c00047
ACS Phys. Chem Au 2024, 4, 660−668

red, Figure 5b). The long-time component in Figure 5b (blue) represents the triplet state. The underlying reasons for these specific lifetimes and their broader implications are explored in the Discussion Section of this paper.

Coherent Nuclear Dynamics

The vibrational coherences observed during transient measurements can provide important details toward understanding the photoexcited behavior of molecular systems.[35] Such coherences can elucidate the structural dynamics and interactions within a molecule and its environment postexcitation, offering insights into the nature of electronic transitions and their coupling to nuclear motions. Figure 6a shows the fs-TA

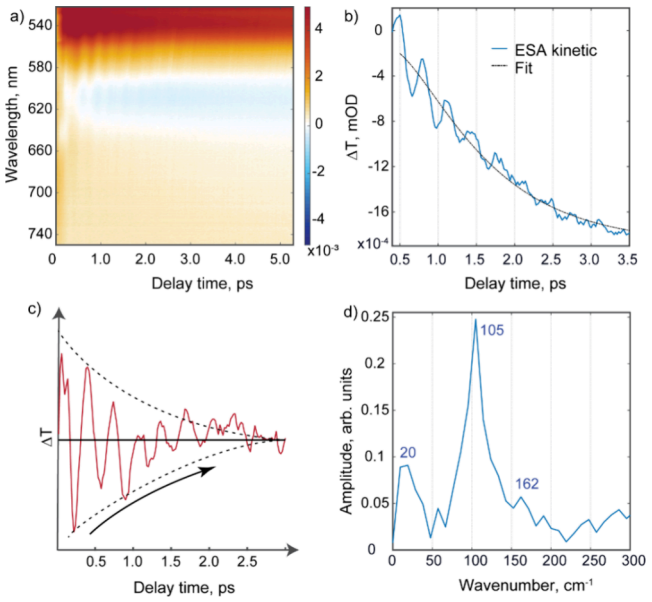

Figure 6. (a) Transient absorption spectrum of the $[Cu(dmp)_2]^+[PF_6]^-$ crystal with a time step of 5 fs, which is a magnified view of the TA spectrum in Figure 3 to clearly show the coherent temporal oscillations. The GSB (red) and ESA (blue) both clearly show oscillatory signatures. (b) Kinetics of the ESA (blue) and a fit (black dashed). (c) Residuals shown in red. (d) Power spectrum highlighting the vibrational frequencies involved.

spectrum for the single crystal, featuring positive bands indicative of the GSB centered at 535 nm, alongside negative bands reflecting ESA centered at 595 nm. The time step for these measurements was set at 5 fs. As already described, the ESA band centered at 595 nm is associated with absorption from the S_1 state to higher energy levels. Oscillations tracing the dynamics of these transient features are distinctly observable across both spectral regions. Figure 6b shows the kinetics of the ESA (blue) at 595 nm, where pronounced oscillations overlay the kinetic decay, indicating the presence of underlying vibrational frequencies. The exponential fit applied to model the kinetic decay is shown as a black dashed line. (The kinetics plots at different band positions in 2D data are presented in the Supporting Information). To analyze the dominant coherent vibrational mode observed, a Fourier transform analysis was conducted on the residuals (shown as a red trace in Figure 6c after excluding decay components. The resulting power spectrum, shown in Figure 6d, exhibits a dominant frequency of approximately 105 cm^{-1}, together with another significant frequency at about 20 cm^{-1}.

To systematically extract vibrational frequencies from various segments of the fs-TA spectrum, global fitting of the data was used. The residuals from this fit, which remove the primary kinetic components, were further Fourier transformed across the full spectrum. The 2D vibrational frequency map generated, which includes both the GSB and ESA regions, is shown in the Supporting Information as Figure S5. Notable low-frequency modes identified include 20 and 105 cm^{-1} modes, along with the 101 cm^{-1} mode attributed in the literature to the "breathing" mode of the complex.[27]

To retrieve the temporal evolution of the ground and excited state frequencies, data from the GSB and ESA regions are further analyzed using wavelet analysis. The details on the analysis are given in the Supporting Information. Figure 7a,b

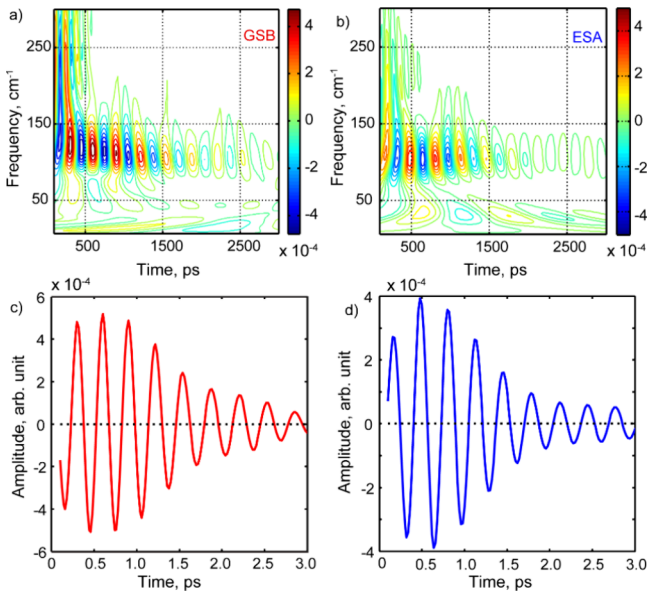

Figure 7. Wavelet analysis of residuals for single crystals from (a) ground state bleach, GSB and (b) excited state absorption. ESA are presented as 2D maps. (c,d) Line sections at 105 cm^{-1} from (a) and (b). The dampling time of the coherences is the same as the ultrafast relaxation dynamics (~430 fs).

shows the spectra obtained after wavelet analysis of the GSB and ESA regions, respectively. Both spectra exhibit pronounced oscillations with a magnitude around 105 cm^{-1}, and the oscillations observed in the GSB and ESA regions are anticorrelated (see also the line sections in Figure 7c,d), highlighting the distinction in vibrational dynamics between the electronic ground and excited states. This anticorrelation is a clear indicator of the distinct and independence of vibrational responses in these different electronic states. Tahara et al. have similarly reported a well-defined vibrational structure in the perpendicular S_1 state in their solution studies. The coherent vibrations in the ESA region align with the vibrational frequencies associated with the perpendicular S_1 state, and this coherence suggests that the ESA region can provide useful insights into specific vibrational modes active in the excited state dynamics of the complex. The observed coherent breathing vibrations is attributed to the compaction forces shortening the Cu−N bond due to the excitation of electron in the HOMO having antibonding character to the LUMO.[27] The ligand-twisting vibrations that induce a flattening motion could not be observed due to the limited bandwidth of the

https://doi.org/10.1021/acsphyschemau.4c00047
ACS Phys. Chem Au 2024, 4, 660−668

pump pulse, which was insufficient to impulsively excite these vibrations.

DISCUSSION

The shorter lifetimes of the perpendicular S_1 state (~430 fs) and the flattened S_1 state (~3.9 ps) within $[Cu(dmp)_2]^+$ crystals, compared to the solution phase, illustrate the impact of lattice-induced stress on the dynamics of excited state populations. The accelerated JT structural distortion observed can be rationalized by the preorganized geometry of the copper complex in the crystalline state, which is preoriented for the formation of Cu(II) following excitation of the MLCT band. Consequently, the system requires less reorganization, with an associated smaller barrier to post photoinduced charge transfer. On the other hand, the reduced lifetime of the flattened S_1 state may be attributed to a combination of accelerated internal conversion to the ground state and expedited triplet formation. The latter process could occur if the flattened S_1 state exhibits a deviation from the square planar geometry. This distortion would lead to variations in spin−orbit coupling (SOC) between the relaxed S_1 and T_1 states in both the crystal and solution phases. Previous studies of $[Cu(dmp)_2]^+$ have indicated that the Franck−Condon (FC) geometry involves an SOC of 300 cm^{-1} between the S_1 and T_1 states.[24] However, poststructural distortion, this SOC value diminishes to about 30 cm^{-1}. In this regard, the accelerated triplet formation is possibly due to hindered planarization of the ligand within the crystal lattice, leading to a relaxed S_1 state in crystals with an increased SOC value. Consequently, the more relaxed S_1 state in crystals, characterized by a partially flattened geometry, would possess a higher energy compared to that of the relaxed S_1 state in solution. Furthermore, our transient analysis suggests stabilization of the T_1 state in crystals compared to the solution phase in DCM, potentially altering the vibronic spin−orbit coupling between these states.

The potential energy diagram in Figure 8 summarizes our main findings and provides an understanding of the photoinduced processes in the $[Cu(dmp)_2]^+$ complex, in both crystalline form and in solution. The molecular geometry of the complex in its ground state (S_0) is prealigned along the coordinate of the photoinduced JT distortion in the crystalline state. On resonant excitation of the MLCT transition to the S_1 state, the oxidation state of copper shifts from Cu(I) to Cu(II), which drives the JT distortion, leading to the relaxation of the S_1 state (S_1^{relax}). Notably, the crystalline form of the complex exhibits faster structural dynamic response compared to the solution form in DCM. This observation can be similarly understood as the extent of JT distortion in the crystalline state may be less pronounced than in the solvated state. This partially relaxed geometry may exhibit higher spin−orbit coupling (SOC), thereby promoting faster triplet formation in crystals. Also, the energy level of the triplet state (T_1) in the crystalline form of the complex is likely to be lower than that in the solution phase. These variations underscore the significant impact of the surrounding matrix on the electronic and dynamic properties of the $[Cu(dmp)_2]^+$ complex, following photoexcitation.

CONCLUSIONS

In this work, we have described time-resolved studies of $[Cu(dmp)_2]^+$ crystals utilizing fs-TA spectroscopy. Within these crystals, the $[Cu(dmp)_2]^+$ complex is found in an entactic state induced by lattice stresses. This state significantly influences the dynamics observed in the excited states. Notably, the photoinduced JT distortion occurs more rapidly in the crystal environment, reducing the lifetime of the FC perpendicular S_1 state to ~430 fs, in contrast to ~730 fs in solution. Our study also details the coherent vibrational dynamics that accompany these structural distortions. Furthermore, the shorter lifetime of the flattened S_1 state (S_1^{relax}) in the crystalline state, at a measured 3.9 ps compared to 11.3 in the solution phase, suggests a larger SOC and more rapid intersystem crossing due to the partially flattened geometry. Thus, our findings demonstrate how lattice-induced entasis can significantly alter the excited state dynamics of Cu(I)-based complexes. The modulation of SOC by lattice stress offers a foundational principle for designing Cu(I)-based metal−organic frameworks tailored for triplet-state-based photocatalysis. By engineering lattice stresses within these frameworks, it is possible to enhance the yield of triplet states, which are crucial for photocatalytic activity in Cu(I)-based systems. Alternatively, these stresses can also be utilized to stabilize singlet states, facilitating singlet photochemistry applications. This study highlights the potential of lattice stress manipulation in tuning the photophysical properties of metal−organic materials for specific catalytic and photochemical functions.

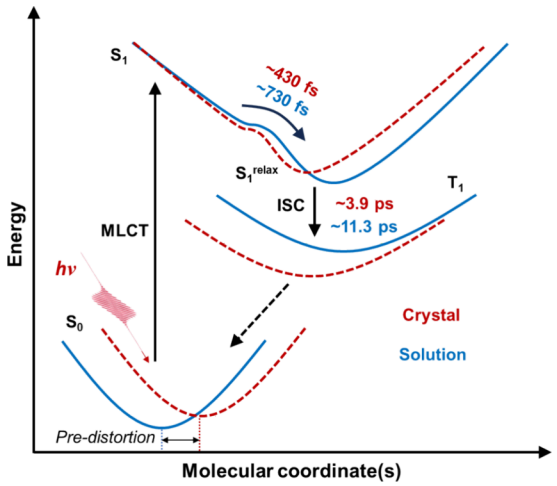

Figure 8. Potential energy scheme summarizing a comparative analysis of the photinduced processes in the $[Cu(dmp)_2]^+[PF_6]^-$ complex in crystalline and solvated states. Molecular geometry of the complex in the ground state, S_0, is preoriented along the photoinduced JT distortion coordinate. On resonant excitation of the MLCT transition to S_1, Cu(I) changes to Cu(II), driving the JT distortion to the S_1^{relax} nuclear configuration. The crystal showed faster dynamics of relaxation and intersystem crossing compared to the solution in DCM. It is speculated that the extent of distortion within the crystal might not be as significant as in the solution due to crystal contacts limiting the degree of relaxation. The energy level of the triplet state (T_1) in the crystal is also likely lower compared with that in solution.

MATERIALS AND METHODS

Synthesis of the $[Cu(dmp)_2]^+[PF_6]^-$ Complex

$[Cu(dmp)_2][PF_6]$ was prepared by the method reported in the literature. The synthesis of the copper complex was systematically prepared by first preparing a 50:50 mixture of water and methanol, which was buffered using acetate to maintain a stable pH. Into this buffered solvent system, sodium hexafluorophosphate ($NaPF_6$) was

https://doi.org/10.1021/acsphyschemau.4c00047
ACS Phys. Chem Au 2024, 4, 660−668

introduced and allowed to dissolve completely. Subsequently, 2,9-dimethyl-1,10-phenanthroline ligand (Merck) and copper(II) sulfate pentahydrate, $CuSO_4{\cdot}5H_2O$ (Merck), were added into the solution mixture. To facilitate the reduction of copper(II) to copper(I), essential for forming the desired copper(I) complex, ascorbic acid was added as a reducing agent. The final step involved the gradual evaporation of methanol under controlled conditions, which led to the precipitation of orange-colored crystals. These crystals represent the copper complex in its solid form, characterized by its distinct coloration, which is indicative of successful complex formation. The obtained crystals were further recrystallized in methanol.

For the optical studies, the crystals of $[Cu(dmp)_2][PF_6]$ were microtomed to a thickness of 400 nm using a LEICA EM UC7 microtome equipped with a DiATOME diamond knife (45°, 3.0 mm).

MicroED

$[Cu(dmp)_2][PF_6]$ crystals were ground into a fine powder between two glass slides and deposited onto a lacey carbon grid (300 mesh, copper) that had been glow discharged for 45 s. Grids were loaded under liquid nitrogen into a CryoARM300 (JEOL) operating at 300 kV. Diffraction movies were recorded using a SerialEM script developed in-house that synchronized slow stage rotation (0.25° s^{-1}) with a K2 summit direct electron detector (GATAN) operated in counting mode.[36,37] Each data set was collected with an electron flux of 0.008 $e^-/Å^2/s$ and rotated over 90° for a total fluence of 2.88 $e^-/Å^2$. Diffraction movies were collected from 15 crystals in Tiff format and converted to MRC by a python script developed in-house, which performed hot pixel removal, gain correction, and data binning. Data reduction (indexing, integration, and scaling) was performed in DIALS.[38,39] The final data set consisted of 5 of the 15 movies merged for phasing by direct methods in Shelxt.[40] The structure was then refined in Shelxl[41] and Olex2.[42]

Femtosecond Transient Absorption Measurements

Transient absorption (TA) measurements for the $[Cu(dmp)_2][PF_6]$ complex in both methanol solution and crystalline forms were carried out using a custom-built TA setup as described in detail previously.[43,44] The system employs a commercial Nd-based PHAROS laser from Light Conversion that emits a fundamental beam at a wavelength of 1030 nm with an output power of 1 W at a frequency of 1 kHz. A beam splitter is used to divide this fundamental beam into pump and probe beams: 20% of the beam is directed through a 3 mm YAG crystal to produce a white light probe beam, while the remaining 80% is used to generate a 343 nm pump beam via a third harmonic generation process. The pump beam's intensity is modulated using a Thorlabs chopper set to 500 Hz, and its energy is adjusted with a series of neutral density filters. At the point of interaction with the sample, the pump and probe beams measure ∼190 and ∼100 μm in diameter, respectively. A 150 mm linear motorized delay stage from Newport is employed to control the timing between the pump and probe beams. The probe spectra at each time delay are captured using a spectrograph (model 9055 from Sciencetech) coupled with a charge-coupled device (CCD) linear image sensor (model S11156-2048-02 from Hamamatsu Photonics). All measurements were conducted at room temperature, 21 °C. Time-resolved absorption spectra were measured with ∼190 fs time resolution. To prevent damage and maintain sample integrity during measurements, the cuvette was mounted on a motorized shaker. For optimal signal-to-noise ratio, 600−800 spectra were averaged for each time delay. The un-normalized absorptions of the $[Cu(dmp)_2]^+$ in solution and crystal at pump excitation wavelength 515 nm are ∼0.22 and ∼0.3 OD, respectively. The photon fluence was accordingly adjusted, $\sim 3 \times 10^{17}$ photons cm^{-2} (solution) and $\sim 2 \times 10^{17}$ photons cm^{-2} (crystal), to achieve approximately the same number of photons absorbed. To ensure data consistency, experiments were repeated on different samples.

The measured TA data was subsequently processed for chirp-correction using MATLAB and then analyzed with Glotran 1.5.1 software for global analysis.[45] The details of the wavelet analysis have been provided in our earlier reports.[46,47] It has also been briefly described in the Supporting Information.

ASSOCIATED CONTENT

Supporting Information

The Supporting Information is available free of charge at https://pubs.acs.org/doi/10.1021/acsphyschemau.4c00047.

Supplementary details on sample characterization including an image of crystals of $[Cu(dmp)_2]^+[PF6]^-$, structure refinement statistics, kinetic plots for TA data, SADS comparisons between solution and crystals, 2D frequency map, and descriptions of the wavelet analysis methods (PDF)

The atomic coordinates elucidated by microED have been deposited in the Cambridge Crystallographic Data Centre with reference number CCDC 2383111. The raw data has been deposited on Zenodo and can be accessed at 10.5281/zenodo.13742284.

AUTHOR INFORMATION

Corresponding Authors

R. J. Dwayne Miller − *The Departments of Chemistry and Physics, University of Toronto, Toronto M5S 3H6, Canada;* orcid.org/0000-0003-0884-0541; Email: dmiller@lphys.chem.utoronto.ca

Ajay Jha − *Rosalind Franklin Institute, Harwell OX11 0QX, United Kingdom; Department of Pharmacology, University of Oxford, Oxford OX1 3QT, United Kingdom;* orcid.org/0000-0002-4489-518X; Email: ajay.jha@rfi.ac.uk

Authors

Vandana Tiwari − *Stanford PULSE Institute, SLAC National Accelerator Laboratory, Menlo Park, California 94025, United States; Department of Chemical Science, Linac Coherent Light Source, SLAC National Accelerator Laboratory, Menlo Park, California 94025, United States*

Marcus Gallagher-Jones − *Rosalind Franklin Institute, Harwell OX11 0QX, United Kingdom*

Hyein Hwang − *European XFEL, Schenefeld 22869, Germany; The Hamburg Centre for Ultrafast Imaging, Hamburg 22761, Germany*

Hong-Guang Duan − *Department of Physics, School of Physical Science and Technology, Ningbo University, Ningbo 315211, China;* orcid.org/0000-0001-6589-0890

Angus I. Kirkland − *Rosalind Franklin Institute, Harwell OX11 0QX, United Kingdom; Department of Materials, University of Oxford, Oxford OX1 3PH, United Kingdom*

Complete contact information is available at: https://pubs.acs.org/10.1021/acsphyschemau.4c00047

Author Contributions

CRediT: **Vandana Tiwari** data curation, formal analysis, visualization, writing - review & editing; **Marcus Gallagher-Jones** data curation, formal analysis, visualization, writing - review & editing; **Hyein Hwang** formal analysis, writing - review & editing; **Hong-Guang Duan** formal analysis, software, writing - review & editing; **Angus I. Kirkland** resources, writing - review & editing; **R. J. Dwayne Miller** funding acquisition, investigation, supervision, writing - review & editing; **Ajay Jha** conceptualization, data curation, formal analysis, investigation, methodology, project administration,

https://doi.org/10.1021/acsphyschemau.4c00047
ACS Phys. Chem Au 2024, 4, 660−668

supervision, validation, visualization, writing - original draft, writing - review & editing.

Notes

The authors declare no competing financial interest.

■ ACKNOWLEDGMENTS

This work was initially supported by the Max Planck Society while the authors (V.T., H.-G.D., R.J.D.M., and A.J.) were at the Max Planck Institute for the Structure and Dynamics of Matter (Hamburg) and was subsequently supported by the Natural Sciences and Engineering Research Council of Cananda (RJDM). H.-G.D. acknowledges funding from NSFC grant no. 12274247 and the Foundation of National Excellent Young Scientist, China. V.T. acknowledges Dr. Hiroki Makita from LBNL, Berkeley, for helpful discussion. The Rosalind Franklin Institute is supported by the EPSRC (V011359/1 (P)) (M.G.J., A.I.K., and A.J.).

■ REFERENCES

(1) Vallee, B. L.; Williams, R. J. Metalloenzymes: the entatic nature of their active sites. *Proc. Natl. Acad. Sci. U.S.A.* **1968**, *59* (2), 498−505.
(2) Williams, R. J. P. Catalysis by metallo-enzymes: The entatic state. *Inorganica Chim. Acta Rev.* **1971**, *5*, 137−155.
(3) Comba, P. Coordination compounds in the entatic state. *Coord. Chem. Rev.* **2000**, *200*−*202*, 217−245.
(4) Stanek, J.; Hoffmann, A.; Herres-Pawlis, S. Renaissance of the entatic state principle. *Coord. Chem. Rev.* **2018**, *365*, 103−121.
(5) Galperin, M. Y.; Koonin, E. V. Divergence and Convergence in Enzyme Evolution. *J. Biol. Inorg. Chem.* **2012**, *287* (1), 21−28.
(6) Das, A.; Hessin, C.; Ren, Y.; Desage-El Murr, M. Biological concepts for catalysis and reactivity: empowering bioinspiration. *Chem. Soc. Rev.* **2020**, *49*, 8840−8867.
(7) Rorabacher, D. B. Electron Transfer by Copper Centers. *Chem. Rev.* **2004**, *104* (2), 651−698.
(8) Lancaster, K. M.; George, S. D.; Yokoyama, K.; Richards, J. H.; Gray, H. B. Type-zero copper proteins. *Nat. chem.* **2009**, *1*, 711−715.
(9) Wittung-Stafshede, P.; Hill, M. G.; Gomez, E.; Di-Bilio, A. J.; Karlsson, G.; Leckner, J.; Winkler, J. R.; Gray, H. B.; Malmström, B. G. Reduction potentials of blue and purple copper proteins in their unfolded states: A closer look at rack-induced coordination. *J. Biol. Inorg. Chem.* **1998**, *3*, 367−370.
(10) Hoffmann, A.; Binder, S.; Jesser, A.; Haase, R.; Flörke, U.; Gnida, M.; Stagni, M. S.; Meyer-Klaucke, W.; Lebsanft, B.; Grünig, L. E.; Schneider, S.; Hashemi, M.; Goos, A.; Wetzel, A.; Rübhausen, M.; Herres-Pawlis, S. Catching an Entatic State—A Pair of Copper Complexes. *Angew. Chem., Int. Ed.* **2014**, *53* (1), 299−304.
(11) Chaka, G.; Sonnenberg, J. L.; Schlegel, H. B.; Heeg, M. J.; Jaeger, G.; Nelson, T. J.; Ochrymowycz, L. A.; Rorabacher, D. B. A Definitive Example of a Geometric "Entatic State" Effect: Electron-Transfer Kinetics for a Copper(II/I) Complex Involving A Quinquedentate Macrocyclic Trithiaether−Bipyridine Ligand. *J. Am. Chem. Soc.* **2007**, *129* (16), 5217−5227.
(12) Garcia, L.; Cisnetti, F.; Gillet, N.; Guillot, R.; Aumont-Nicaise, M.; Piquemal, J.-P.; Desmadril, M.; Lambert, F.; Policar, C.; et al. Entasis through Hook-and-Loop Fastening in a Glycoligand with Cumulative Weak Forces Stabilizing CuI. *J. Am. Chem. Soc.* **2015**, *137* (3), 1141−1146.
(13) Stanek, J.; Sackers, N.; Fink, F.; Paul, M.; Peters, L.; Grunzke, R.; Hoffmann, A.; Herres-Pawlis, S. Copper Guanidinoquinoline Complexes as Entatic State Models of Electron-Transfer Proteins. *Chem. - Eur. J.* **2017**, *23* (62), 15738−15745.
(14) Hernandez-Perez, A. C.; Collins, S. K. Heteroleptic Cu-Based Sensitizers in Photoredox Catalysis. *Acc. Chem. Res.* **2016**, *49* (8), 1557−1565.
(15) McCusker, C. E.; Castellano, F. N. Design of a Long-Lifetime, Earth-Abundant, Aqueous Compatible Cu(I) Photosensitizer Using Cooperative Steric Effects. *Inorg. Chem.* **2013**, *52* (14), 8114−8120.
(16) Dahl, E. W.; Szymczak, N. K. Hydrogen Bonds Dictate the Coordination Geometry of Copper: Characterization of a Square-Planar Copper(I) Complex. *Angew. Chem., Int. Ed.* **2016**, *55* (9), 3101−3105.
(17) Garcia, L.; Maisonneuve, S.; Xie, J.; Guillot, R.; Dorlet, P.; Rivière, E.; Desmadril, M.; Lambert, F.; Policar, C. Sugars to Control Ligand Shape in Metal Complexes: Conformationally Constrained Glycoligands with a Predetermination of Stereochemistry and a Structural Control. *Inorg. Chem.* **2010**, *49* (16), 7282−7288.
(18) Dicke, B.; Hoffmann, A.; Stanek, J.; Rampp, M. S.; Grimm-Lebsanft, B.; Biebl, F.; Rukser, D.; Maerz, B.; Göries, D.; Naumova, M.; Biednov, M.; Neuber, G.; Wetzel, A.; Hofmann, S. M.; Roedig, P.; Meents, A.; Bielecki, J.; Andreasson, J.; Beyerlein, K. R.; Chapman, H. N.; Bressler, C.; Zinth, W.; Rübhausen, M.; Herres-Pawlis, S. Transferring the entatic-state principle to copper photochemistry. *Nat. Chem.* **2018**, *10*, 355−362.
(19) Gimeno, L.; Phelan, B. T.; Sprague-Klein, E. A.; Roisnel, T.; Blart, E.; Gourlaouen, C.; Chen, L. X.; Pellegrin, Y. Bulky and Stable Copper(I)-Phenanthroline Complex: Impact of Steric Strain and Symmetry on the Excited-State Properties. *Inorg. Chem.* **2022**, *61* (19), 7296−7307.
(20) Le Poul, N.; Campion, M.; Izzet, G.; Douziech, B.; Reinaud, O.; Le Mest, Y. Electrochemical Behavior of the Tris(pyridine)−Cu Funnel Complexes: An Overall Induced-Fit Process Involving an Entatic State through a Supramolecular Stress. *J. Am. Chem. Soc.* **2005**, *127* (15), 5280−5281.
(21) McMillin, D. R.; Buckner, M. T.; Ahn, B. T. A light-induced redox reaction of bis(2,9-dimethyl-1,10-phenanthroline)copper(I). *Inorg. Chem.* **1977**, *16* (4), 943−945.
(22) Saha, A.; Nia, S. S.; Rodríguez, J. A. Electron Diffraction of 3D Molecular Crystals. *Chem. Rev.* **2022**, *122* (17), 13883−13914.
(23) Scaltrito, D. V.; Thompson, D. W.; O'Callaghan, J. A.; Meyer, G. J. MLCT excited states of cuprous bis-phenanthroline coordination compounds. *Coord. Chem. Rev.* **2000**, *208*, 243−266.
(24) Siddique, Z. A.; Yamamoto, Y.; Ohno, T.; Nozaki, K. Structure-Dependent Photophysical Properties of Singlet and Triplet Metal-to-Ligand Charge Transfer States in Copper(I) Bis(diimine) Compounds. *Inorg. Chem.* **2003**, *42*, 6366−6378.
(25) Chen, L. X.; Shaw, G. B.; Novozhilova, I.; Liu, T.; Jennings, G.; Attenkofer, K.; Meyer, G. J.; Coppens, P. MLCT State Structure and Dynamics of a Copper(I) Diimine Complex Characterized by Pump−Probe X-ray and Laser Spectroscopies and DFT Calculations. *J. Am. Chem. Soc.* **2003**, *125* (23), 7022−7034.
(26) Samia, A. C. S.; Cody, J.; Fahrni, C. J.; Burda, C. The Effect of Ligand Constraints on the Metal-to-Ligand Charge-Tranfer Relaxation Dynamics of Copper(I)−Phenanthroline Complexes: A Comparative Study by Femtosecond Time-Resolved Spectroscopy. *J. Phys. Chem. B* **2004**, *108* (2), 563−569.
(27) Iwamura, M.; Takeuchi, S.; Tahara, T. Real-Time Observation of the Photoinduced Structural Change of Bis(2,9-dimethyl-1,10-phenanthroline)copper(I) by Femtosecond Fluorescence Spectroscopy: A Realistic Potential Curve of the Jahn−Teller Distortion. *J. Am. Chem. Soc.* **2007**, *129* (16), 5248−5256.
(28) Iwamura, M.; Takeuchi, S.; Tahara, T. Ultrafast Excited-State Dynamics of Copper(I) Complexes. *Acc. Chem. Res.* **2015**, *48* (3), 782−791.
(29) Iwamura, M.; Watanabe, H.; Ishii, K.; Takeuchi, S.; Tahara, T. Coherent Nuclear Dynamics in Ultrafast Photoinduced Structural Change of Bis(diimine)copper(I) Complex. *J. Am. Chem. Soc.* **2011**, *133* (20), 7728−7736.
(30) Shaw, G. B.; Grant, C. D.; Shirota, H.; Castner, E. W.; Meyer, G. J.; Chen, L. X. Ultrafast Structural Rearrangements in the MLCT Excited State for Copper(I) bis-Phenanthrolines in Solution. *J. Am. Chem. Soc.* **2007**, *129* (7), 2147−2160.

https://doi.org/10.1021/acsphyschemau.4c00047
ACS Phys. Chem Au 2024, 4, 660−668

(31) Cuttell, D. G.; Kuang, S.-M.; Fanwick, P. E.; McMillin, D. R.; Walton, R. A. Simple Cu(I) Complexes with Unprecedented Excited-State Lifetimes. *J. Am. Chem. Soc.* **2002**, *124* (1), 6−7.
(32) Mara, M. W.; Fransted, K. A.; Chen, L. X. Interplays of excited state structures and dynamics in copper(I) diimine complexes: Implications and perspectives. *Coord. Chem. Rev.* **2015**, *282*−*283*, 2−18.
(33) van Stokkum, I. H. M.; Larsen, D. S.; van Grondelle, R. Global and target analysis of time-resolved spectra. *Biochim. Biophys. Acta, Bioenerg.* **2004**, *1657* (2−3), 82−104.
(34) Ruckebusch, C.; Sliwa, M.; Pernot, P.; de Juan, A.; Tauler, R. Comprehensive data analysis of femtosecond transient absorption spectra: A review. *J. Photochem. Photobiol. C: Photochem. Rev.* **2012**, *13* (1), 1−27.
(35) Scholes, G. D.; Fleming, G. R.; Chen, L. X.; Aspuru-Guzik, A.; Buchleitner, A.; Coker, D. F.; Engel, G. S.; van Grondelle, R.; Ishizaki, A.; Jonas, D. M.; Lundeen, J. S.; McCusker, J. K.; Mukamel, S.; Ogilvie, J. P.; Olaya-Castro, A.; Ratner, M. A.; Spano, F. C.; Whaley, K. B.; Zhu, X. Using coherence to enhance function in chemical and biophysical systems. *Nature* **2017**, *543*, 647−656.
(36) Gallagher-Jones, M.; Bustillo, K. C.; Ophus, C.; Richards, L. S.; Ciston, J.; Lee, S.; Minor, A. M.; Rodriguez, J. A. Atomic structures determined from digitally defined nanocrystalline regions. *IUCrJ.* **2020**, *7* (3), 490−499.
(37) Hattne, J.; Clabbers, M. T. B.; Martynowycz, M. W.; Gonen, T. Electron counting with direct electron detectors in MicroED. *Structure* **2023**, *31* (12), 1504−1509.
(38) Winter, G.; Waterman, D. G.; Parkhurst, J. M.; Brewster, A. S.; Gildea, R. J.; Gerstel, M.; Fuentes-Montero, L.; Vollmar, M.; Michels-Clark, T.; Young, I. D.; Sauter, N. K.; Evans, G. DIALS: implementation and evaluation of a new integration package. *Acta Crystallogr. D* **2018**, *74* (2), 85−97.
(39) Clabbers, M. T. B.; Gruene, T.; Parkhurst, J. M.; Abrahams, J. P.; Waterman, D. G. Electron diffraction data processing with DIALS. *Acta Crystallogr. D* **2018**, *74* (6), 506−518.
(40) Sheldrick, G. SHELXT - Integrated space-group and crystal-structure determination. *Acta Crystallogr. A* **2015**, *71* (1), 3−8.
(41) Sheldrick, G. Crystal structure refinement with SHELXL. *Acta Crystallogr. C* **2015**, *71* (1), 3−8.
(42) Dolomanov, O. V.; Bourhis, L. J.; Gildea, R. J.; Howard, J. A. K.; Puschmann, H. OLEX2: a complete structure solution, refinement and analysis program. *J. Appl. Crystallogr.* **2009**, *42*, 339−341.
(43) Hwang, H.; Tiwari, V.; Duan, H.-G.; Bittmann, S. F.; Tellkamp, F.; Jha, A.; Miller, R. J. D. Two-dimensional confinement for generating thin single crystals for applications in time-resolved electron diffraction and spectroscopy: an intramolecular proton transfer study. *Chem. Commun.* **2022**, *58*, 9774−9777.
(44) Yan, Y.; Liu, C.; Yang, Y.; Hu, G.; Tiwari, V.; Jiang, D.; Peng, W.; Jha, A.; Duan, H.-G.; Tellkamp, F.; Ding, Y.; Shi, W.; Yuan, S.; Miller, D.; Ma, W.; Zhao, J. Fundamental Flaw in the Current Construction of the TiO2 Electron Transport Layer of Perovskite Solar Cells and Its Elimination. *ACS Appl. Mater. Interfaces* **2021**, *13* (33), 39371−39378.
(45) Snellenburg, J. J.; Laptenok, S. P.; Seger, R.; Mullen, K. M.; Stokkum, I. H. M. v. Glotaran: a Java-based Graphical User Interface for the R-package TIMP. *J. Stat. Software* **2012**, *49*, 1−22.
(46) Duan, H.-G.; Tiwari, V.; Jha, A.; Berdiyorov, G. R.; Akimov, A.; Vendrell, O.; Nayak, P. K.; Snaith, H. J.; Thorwart, M.; Li, Z.; Madjet, M. E.; Miller, R. J. D. Photoinduced Vibrations Drive Ultrafast Structural Distortion in Lead Halide Perovskite. *J. Am. Chem. Soc.* **2020**, *142* (39), 16569−16578.
(47) Jha, A.; Zhang, P. P.; Tiwari, V.; Chen, L.; Thorwart, M.; Miller, R. J. D.; Duan, H. G. Unraveling quantum coherences mediating primary charge transfer processes in photosystem II reaction center. *Sci. Adv.* **2024**, *10* (10), No. eadk1312.

https://doi.org/10.1021/acsphyschemau.4c00047
ACS Phys. Chem Au 2024, 4, 660−668